

RESEARCH PAPER

Facile Synthesis of Fe/ZnO Hollow Spheres Nanostructures by Green Approach for the Photodegradation and Removal of Organic Dye Contaminants in Water

Seyed Mohsen Mousavi*, Mahshid Golestaneh

Department of Chemistry, Farhangian University, Tehran, P.O. Box 19989-63341, Islamic Republic of Iran

ARTICLE INFO

Article History:

Received 29 July 2020

Accepted 14 October 2020

Published 01 January 2021

Keywords:

Dyes

Fe/ZnO hollow sphere

Green synthesizes

Nanostructures

Photocatalytic degradation

ABSTRACT

In this research, a facile and clean sonochemical synthesis was described for Fe/ZnO hollow spheres nanostructures as high-efficiency UV-Vis light photocatalyst through an environmentally-friendly procedure. X-ray diffraction (XRD), Fourier-transform infrared spectroscopy (FT-IR), and field-emission scanning electron microscopy (FE-SEM) were utilized for the investigation of the produced Fe/ZnO hollow spheres nanostructures. Then, the photocatalytic activities of the catalysts were evaluated on the degradation of Methylene Blue and Congo Red in an aqueous solution under both UV and visible light irradiation ($\lambda > 420$ nm). Also, to illustrate the influence of morphologies on the degradation of these organic dyes, the Fe/ZnO nanostructures with the wood-like, flower-like, rod-like, and nanoparticle morphologies were synthesized and the photocatalyst efficiency of them was determined. The results confirmed that the Fe/ZnO hollow spheres have significant photocatalytic activity compared to other morphologies and could be used as outstanding potential photocatalyst materials for removing dye pollutants from water.

How to cite this article

Mousavi S.M., Golestaneh M. Facile Synthesis of Fe/ZnO Hollow Spheres Nanostructures by Green Approach for the Photodegradation and Removal of Organic Dye Contaminants in Water. J Nanostruct, 2021; 11(1): 20-30. DOI: 10.22052/JNS.2021.01.003

INTRODUCTION

Nowadays, water pollution has become one of the serious problems facing the human race [1]. Among water contaminants, synthetic dyes in the sewage of different industries are usually toxic and may including non-biodegradable dye molecules that are damaging to the environment [2]. Therefore, because of the non-biodegradability and ruinous nature of synthetic dyes, the treatment of these pollutants is necessary for defending the environment, ecosystem, and human life [3,4]. Different methods such as adsorption [5], solvent extraction [6], biodegradation [7], ozone [8] and, Photocatalysis [9, 10] have been applied for wastewater treatment. Among these methods, the photocatalytic method for its unique

advantages such as using sunlight, high efficiency, simple equipment, low energy consumption, and complete mineralization of pollutants without secondary pollution has become a focus on research in recent years [11, 12]. The development of green and environmentally-friendly photocatalyst with high stability, greater photocatalytic activity, and low cost has become an arduous and hot situation in the study of photocatalytic methods [13, 14].

ZnO is generally considered a substitute photocatalyst for a large surface area, cheap, non-toxic property, and broadband-gap (~ 3.37 eV) for use in solar cells, biosensors, photocatalysis, photodiodes, gas sensors, transistors, and chemical sensors [15-17]. But, ZnO cannot be applied for direct solar irradiation because of

* Corresponding Author Email: smm4566@cfu.ac.ir

its rapid recombination of charge carriers, and lower stability because of photocorrosion [18, 19]. Different approaches were developed to reduce the recombination rate of photogenerated electrons and holes in ZnO. Among these methods, ZnO-based heterostructure with the electron scavenging agents such as metals, metal oxides, or organic molecules has received much attention recently because it can provide a potential driving force to achieve efficient separation of electron-hole pairs and faster carrier migration [20, 21].

The efforts to gain specific morphologies of nanomaterials for advanced applications have become one of the major goals of materials science in recent years [22]. Hollow structures and carbon hollow spheres are among these special morphologies that exhibit lower density, larger area, and specific optical properties [23]. Use of the eco-friendly raw materials (any of the saccharides and some biomass) and easy adjustment of absorption or annealing of metal ions on the surface functional groups in the carbon hollow spheres result of the high-performance photocatalytic properties of these nanostructures [24].

In this study, the Fe/ZnO hollow spheres were synthesized via an environment-friendly, simple, and energy-saving sonochemical method and used as photocatalyst. For this, fructose was used for the synthesis of the templates of carbon microspheres. Then, these templates remove spontaneously to form hollow-cores. For the exploration of the photocatalytic performance of these hollow spheres, the Congo Red (CR) and Methylene Blue (MB) were used that usually applied as a model pollutant to investigate the dye removal ability of photocatalyst [25]. The photodegradation of these dyes in the presence of synthesized nanostructure photocatalyst was studied and the effects of different parameters on the CR and MB degradation were investigated. To compare the influence of morphologies on the degradation of CR and MB, the Fe/ZnO nanostructures with different methods were synthesized and the photocatalyst efficiency of them on the degradation of CR and MB was examined.

MATERIALS AND METHODS

All chemicals were analytical grade from Merck and used as received without any purification. Fructose, zinc (II) acetate dihydrate (Merck, 99.9%),

iron (II) acetate tetrahydrate (Merck, 99.9%).

Characterizations

The X-ray diffraction (XRD) measurements were done using a Philips Expert Pro MPD, Cu-K α radiation ($\lambda = 1.54056 \text{ \AA}$). The surface morphology of producing samples was determined using a field emission scanning electron microscope (FE-SEM) (Mira TESCAN) with a gold coating. The energy dispersive spectrometry (EDS) analysis of samples was investigated using an XL30, Philips microscope. The UV-Vis spectrometer model Shimadzu UV 2100 was used to obtain the UV-Vis absorption spectra. The FTIR spectra of the samples were recorded on a Nicolet Fourier Transform, Nicolet 100 spectrometer in the range of 400–4000 cm^{-1} . Deionized water was used for all experiments.

Green synthesis of carbon spheres

The preparation method of carbon microspheres is given in our previous work [26]. Briefly, 10 g fructose dissolved in 100 ml deionized water until a clear solution was achieved. Then, this solution was moved into a 150 ml Teflon-lined autoclave and hold at 160 °C for 4 h. The suspension was then cooled down to room temperature and the carbon spheres were separated, washed several times with deionized water. Finally, carbon microspheres dried at 80 °C for 2 h to evaporate the water.

Ultrasound-assisted synthesis of ZnO hollow sphere

2.2 g of zinc (II) acetate dihydrate was dissolved in 50 ml of deionized water (solution A). 1.0 g of carbon hollow spheres (as templates) was dispersed in 20 ml of deionized water (solution B). Next, the solution B was added to solution A in the ultrasonic bath and at room temperature (followed by stirring for 2 h). Afterward, the centrifuged mixture was filtered and washed with deionized water. Finally, the collected material was calcined in a furnace that was adjusted at 500 °C (6 h) until ZnO hollow spheres were formed.

Ultrasound-assisted synthesis of Fe-doped ZnO hollow sphere

To synthesize x-Fe/ZnO (x = 0, 3, 5, and 10 wt% Fe) hollow spheres, two solutions were prepared as follows: firstly, 2.0 g zinc (II) acetate dihydrate with an appropriate amount of iron (II) acetate tetrahydrate (according to required

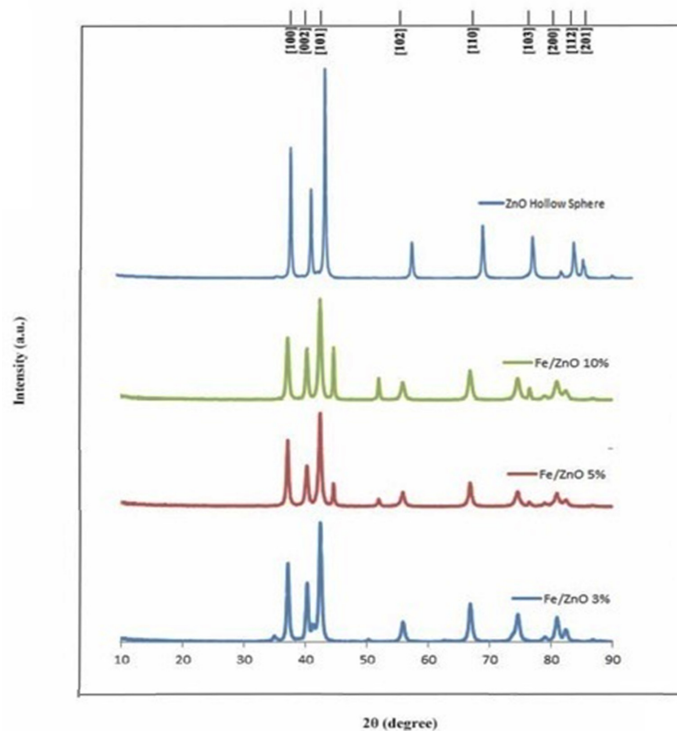


Fig. 1. XRD patterns of the x-Fe/ZnO hollow sphere (x = 0, 3, 5, and 10 wt% Fe)

weight percent) were mixed and dissolved in 40 ml of deionized water (solution A). Secondly, 1.0 g of as-prepared carbon hollow spheres was homogeneously dispersed in 20 ml of deionized water (solution B). Afterward, solution B was added to solution A in the ultrasonic bath at room temperature and dispersed for 1 h. The obtained suspension was then dried under ambient conditions over 24 h and then was washed with deionized water. The product was heated from room temperature to 500 °C with a rate of 1 °C min⁻¹ and kept at 500 °C for 2 h. Finally, Fe/ZnO hollow spheres with a white to reddish-white color were synthesized. The obtained hollow spheres were eventually occupied as a photocatalyst to decay the MB and CR pollutants.

The photocatalytic experiment of Fe/ZnO hollow spheres

The photocatalytic performance of x-Fe/ZnO hollow spheres was evaluated through the degradation of CR and MB as the target pollutants under visible and UV light irradiations. The irradiation was created with a 30W Philips UV lamp with UV-light wavelength of 253.7 nm and/or a 400 W high-pressure mercury-vapor

lamp (providing visible light ≥ 300 nm). 25.0 mg of the photocatalyst (i.e., the pure ZnO or x-Fe/ZnO hollow spheres) was weighed and placed into 50 ml of the CR and MB solutions with the concentration of 20 ppm. Before irradiation, the suspension was magnetically stirred in darkness for 30 min to confirm an adsorption-desorption equilibrium. At a regular time interval of 30 min, 3 ml of the suspension was gathered, centrifuged and decolorization of dye solutions was measured using a UV-Vis spectrophotometer. The change of CR and MB absorbance was utilized to monitor the amount of degradation of these dyes.

RESULTS AND DISCUSSION

Characterization of Fe/ZnO hollow spheres

Fig. 1 presents the X-ray diffraction patterns of pure Zn and x-Fe/ZnO hollow sphere products (0, 3, 5, and 10 wt% Fe). All of the indexed peaks in the spectra are well confirmed by that of the hexagonal wurtzite structure of the ZnO hollow sphere with lattice constants of $a = b = 3.25$ Å and $c = 5.207$ Å (JCPDS Card No. 36-1451). The great crystallinity of the synthesized samples is well illustrated by their relatively intense and strong peaks. The peaks specified by XRD analysis for all

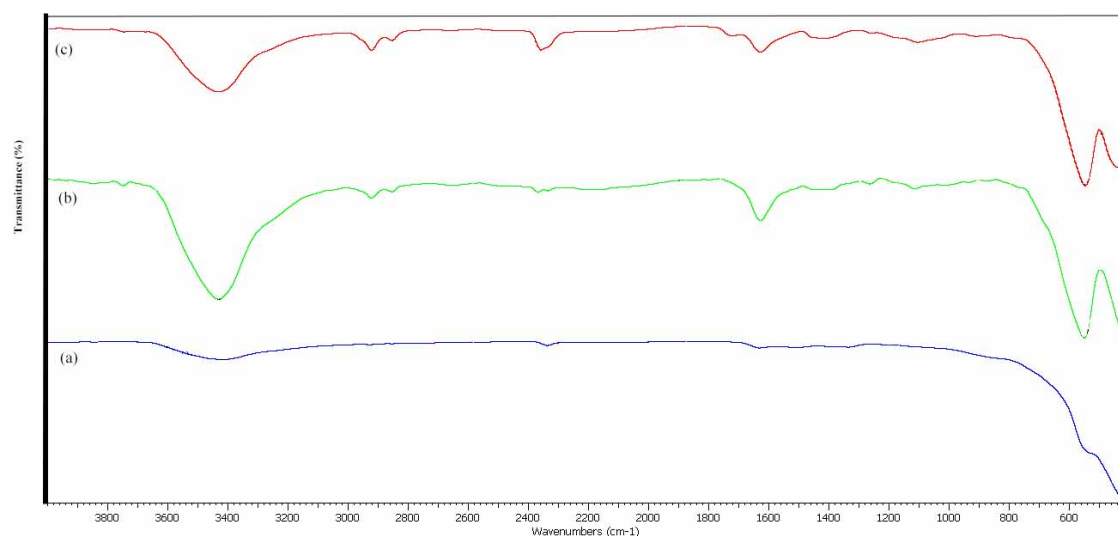


Fig. 2. FTIR spectra of the Fe/ZnO hollow sphere (a = 10, b=5, c=3) wt% Fe.

samples along with the matching materials in Fig. 1.

FT-IR results were used to confirm the chemical interactions and bonding structures of the synthesis products. FT-IR is extremely reactive versus the vibrations in the metal-oxygen bonds. Because of the existence of inter-atomic vibrations in metal oxides, the absorption bands related to stretching of M-O were observed in the region below 1000 cm^{-1} . Therefore, the sharp bands in this region confirmed that the metal oxide was formed [27]. FT-IR spectra of the synthesis Fe/ZnO hollow spheres were shown in Fig. 2. The broadband at 540 cm^{-1} is attributable to the stretching vibrations of Zn-O, while the band at 430 cm^{-1} is corresponding to the Fe-O stretching. The observed peaks at 3438 , 1631 , and 1381 cm^{-1} could be related to the adsorption of water in the produced hollow spheres [28]. Also, no organic species were formed during the preparation of Fe-ZnO hollow spheres; therefore, FT-IR spectra agree with XRD patterns.

The morphology of the x-Fe/ZnO hollow spheres (x = 3, 5, 10, 15 wt% Fe) synthesized via the ultrasonic method was investigated using FE-SEM. As seen in Fig. 3 with increasing the amount of Fe, the morphologies of particles have shifted from a situation of more spherical to a situation of more spiral. Also, with increasing the amount of Fe to more than 10% wt Fe, the spherical shell turns into a thinner and thinner shell, and within the cooling procedure will partially or completely collapse [29]. Due to the existing vacant space in

the center of these nanostructures, a large surface area in Fe/ZnO hollow spheres would be attained.

Elemental analysis of the prepared Fe/ZnO hollow spheres was performed using EDAX spectroscopy. Fig. 4 exhibits the chemical composition of Fe/ZnO hollow spheres, in which the results are agreeing with those of XRD patterns and confirmed the presence of elements Zn, Fe, and O in the synthesized samples. On the other hand, the presence of Fe ions in these hollow spheres was proved. Fig. 4 a-c corresponding to 3, 5, and 10 wt% Fe, respectively. The additionally detected peaks in the EDAX spectra could be originated from the Au element employed in the EDAX stage when the sample sputter was coated. Also, the weight ratio obtained from EDAX spectra was almost in agreement with the initial amounts used to prepare the samples. The Zn and O ions concentration (wt.%) were found to be approximately 92 % and 8%, respectively.

Investigation of the photocatalytic activity

To evaluate the photocatalytic performance of synthesis nanostructured catalysts, the degradation of MB and CR in aqueous solution under both UV and visible light irradiations ($> 420\text{ nm}$) was performed. The origin of the photocatalytic procedure is based on the generation of electron-hole pairs with radiation. The hydroxyl free radical (OH^\cdot), which originated from the oxidation of OH^- or H_2O and produced the electron-hole pairs in the presence of oxygen, could be the driving force of the photocatalytic procedure through degrading

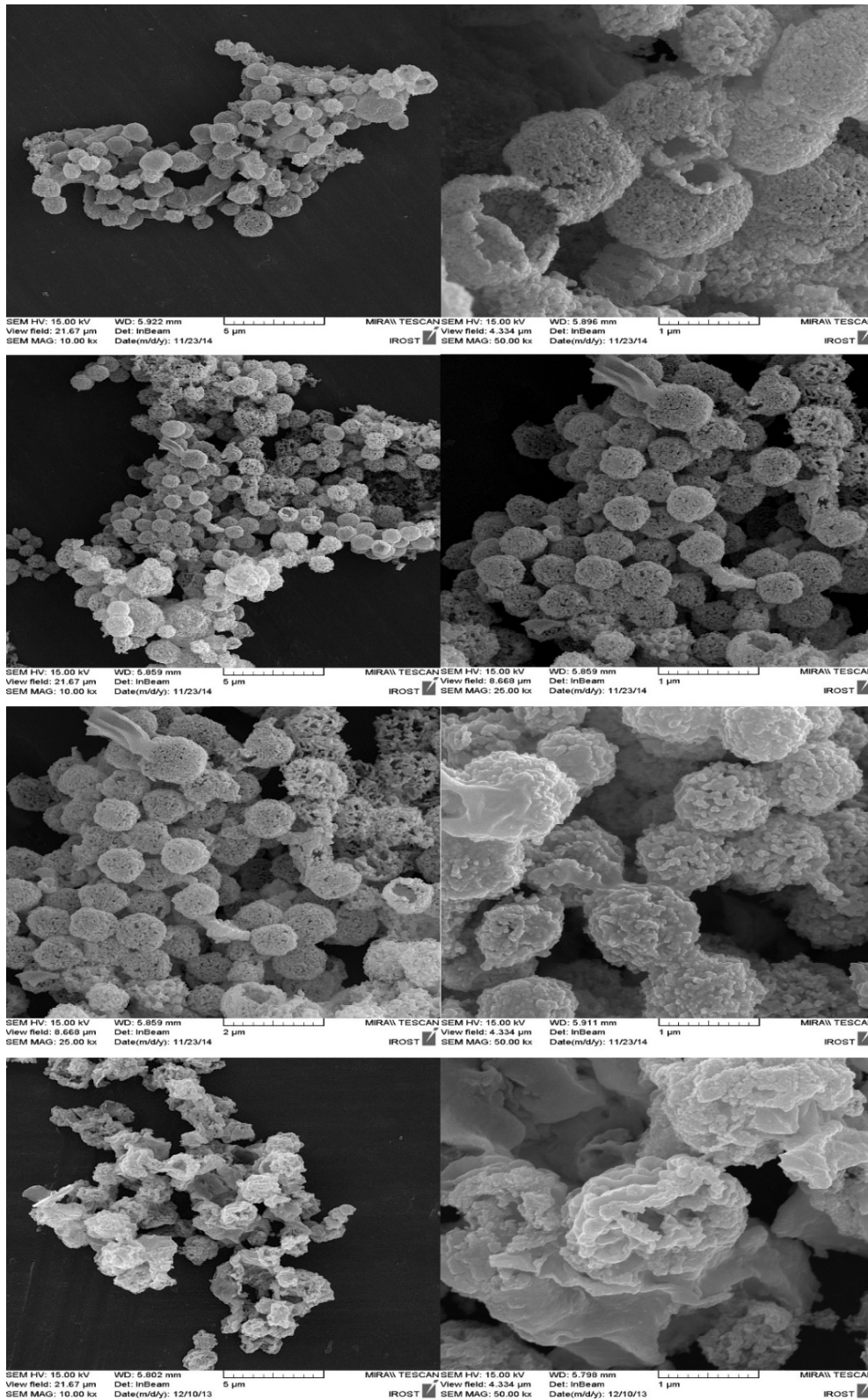


Fig. 3. FE-SEM images of the x-Fe/ZnO hollow sphere (x = 3 (a,b), x=5 (c,d), x=10 (e,f), x = 15 (g,h) % wt Fe

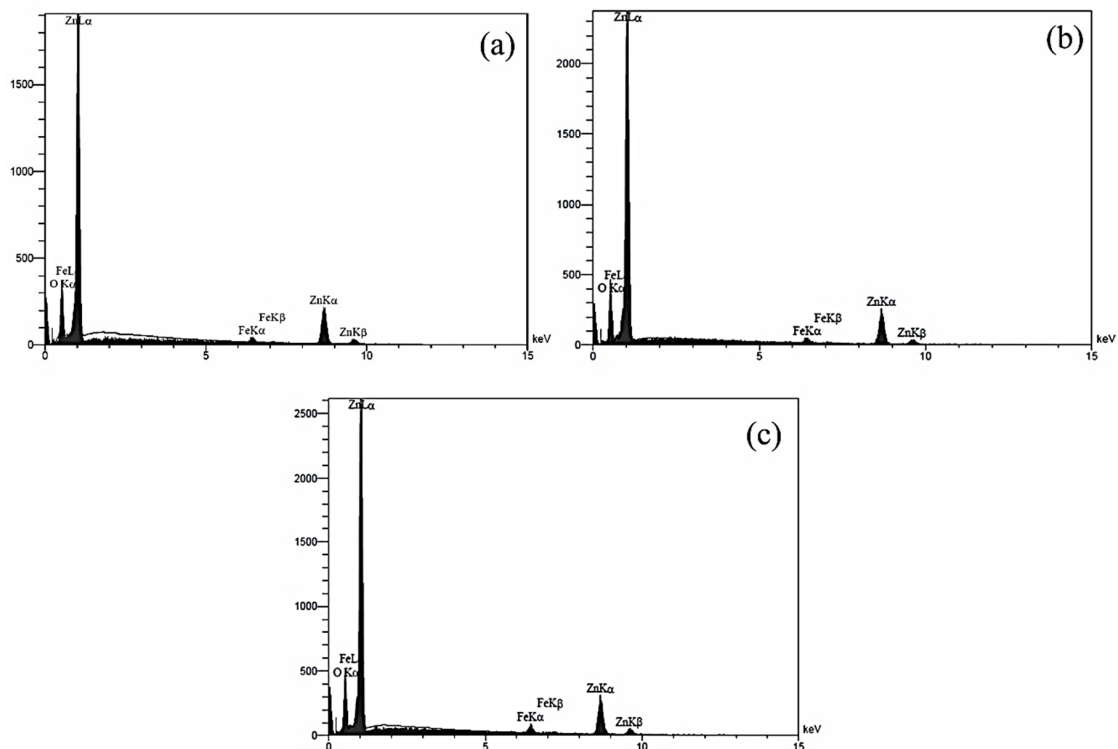


Fig. 4. EDAX analysis of the x-Fe/ZnO hollow spheres that Fe weight content (x) was (a) 3, (b) 5, and (c) 10 % wt.

the conjugated bonds existent in the organic pollutants [30].

Based on the unique structural and morphological characteristics of Fe/ZnO hollow spheres, the photocatalytic activity for CR and MB degradation is examined. The degradation of CR and MB dyes under UV-vis light irradiation to determine the photocatalytic activity of pure ZnO spheres, and x-Fe/ZnO hollow spheres (x = 0, 3, 5, and 10 wt %) were presented in Figs. 5, 6.

As can be seen in Figs. 5a and 6a in the presence of ZnO hollow spheres under UV light irradiation after 35 min, the degradation of CR and MB was 79% and 74%, respectively. The presence of all Fe/ZnO hollow spheres samples displays higher photocatalytic activity than pure ZnO spheres. The photocatalyst effect of x-Fe/ZnO enhanced by the increase of wt% of Fe in the catalyst so that in the presence of 10% wt Fe, the elimination of CR and MB increased to 99% and 83%, respectively.

Figs. 5b and 6b showed the degradation of CR and MB under visible light irradiations in the presence of pure ZnO and Fe/ZnO hollow spheres. After 60 min, the ZnO catalyst could be eliminated the 94% and 76% of the CR and MB, respectively. These amounts increased in the presence of Fe/

ZnO as the photocatalyst, so that the degradation of the CR and MB increased to 97% and 80%, respectively when the amount of Fe reached 10% wt.

According to the literature, morphology and surface area are important for improving the photocatalytic property [31]. Therefore, we prepared Fe/ZnO nanostructures using other methods, and then, the photocatalytic activity of these nanostructures in the degradation of CR and MB was examined and compared with Fe/ZnO hollow spheres. Fig. 7 exhibits the FE-SEM images of Fe/ZnO nanostructures with different morphologies synthesized by microwave, solvothermal, hydrothermal and, sol-gel. These morphologies consist of flower-like, wood-like, rod-like, and nanoparticles, respectively.

A comparison of the performance of the Fe/ZnO hollow sphere with other morphological nanostructures on the degradation of the CR and MB under UV irradiation was shown in Fig. 8a and 8b, respectively. It was found that Fe/ZnO hollow sphere with 99% efficiency was more effective than other morphologies (Fig. 8a). The performance of wood-like, flower-like, rod-like, and nanoparticle morphologies under UV irradiation after 35

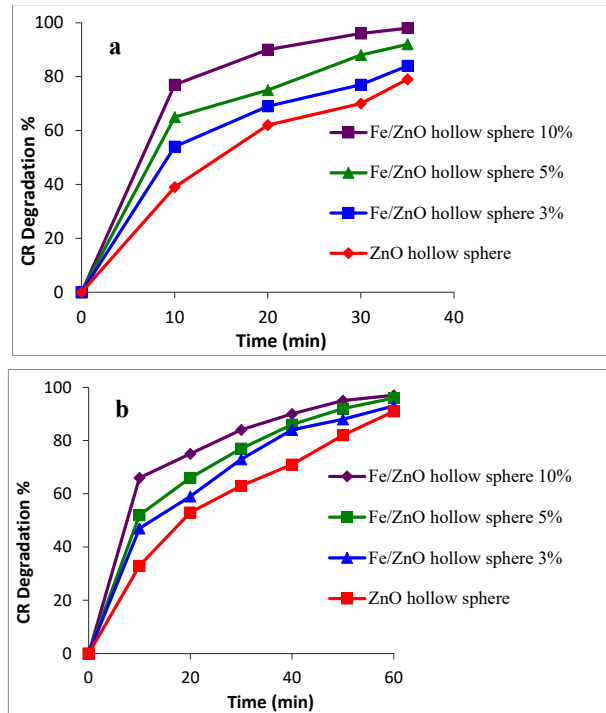


Fig. 5. Photodegradation of CR in the presence of x-Fe/ZnO hollow spheres (x= 0, 3, 5, 10 wt%) at (a) UV and (b) visible irradiation.

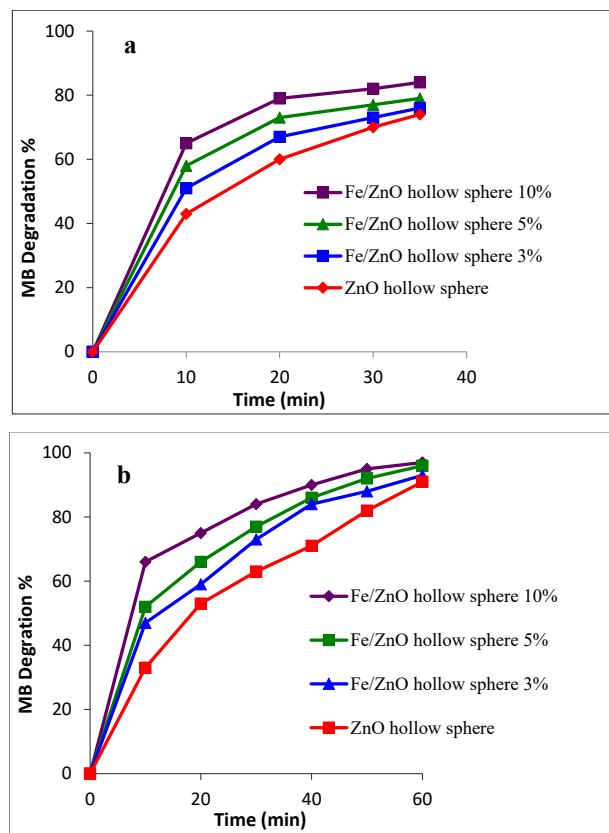


Fig. 6. Photodegradation of MB in the presence of x-Fe/ZnO hollow spheres (x= 0, 3, 5, 10 wt%) at (a) UV and (b) visible irradiation.

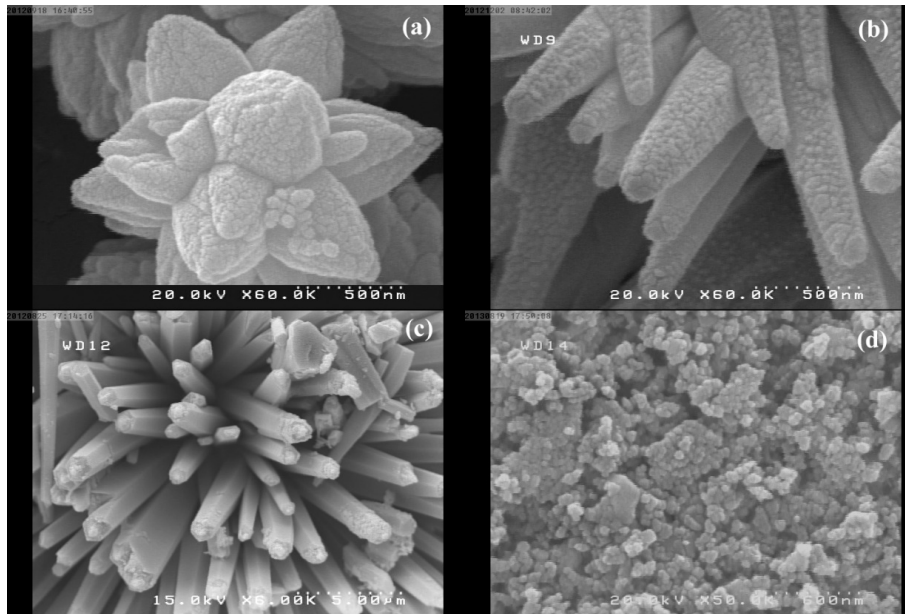


Fig. 7 SEM images of the Fe/ZnO nanostructures synthesized via (a) microwave, (b) solvothermal, (c) hydrothermal and (d) sol-gel.

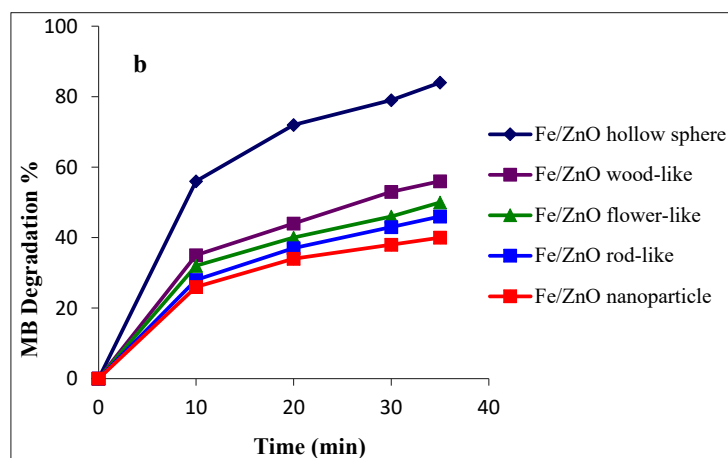
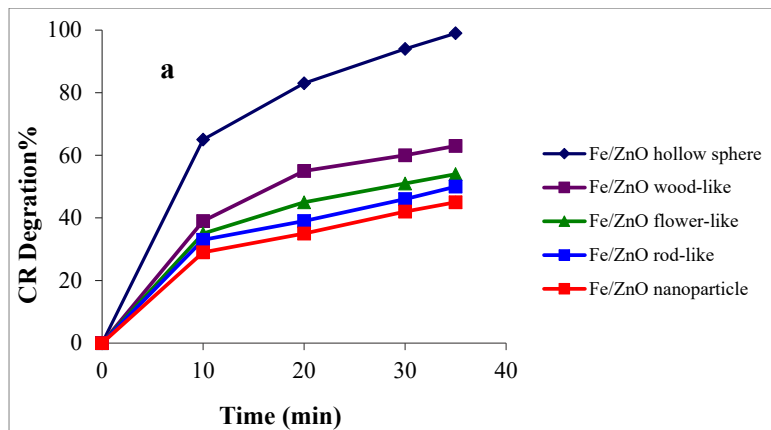


Fig. 8 Photodegradation of CR (a) and MB (b) in the presence of x-Fe/ZnO nanostructures (x = 10 % wt Fe) with different morphologies under UV light

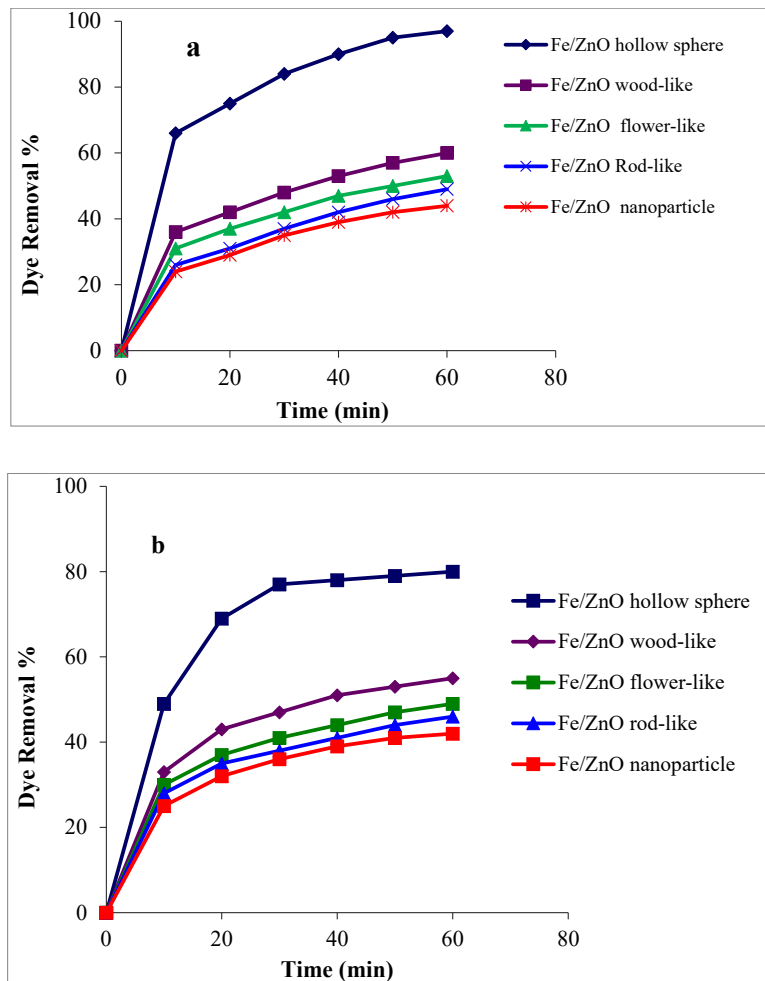


Fig. 9 Photodegradation of CR (a) and MB (b) in the presence of x-Fe/ZnO nanostructures (x = 10% wt Fe) with different morphologies under Visible light

min was found to be 63%, 54%, 50%, and 45%, respectively. Fig. 8b is shown the efficiency of synthesized nanostructures on the degradation of MB under UV irradiation. As can be seen after 35 min, the Fe/ZnO efficiency for MB degradation was 84%, which was much higher than the other morphologies. The efficiency of wood-like, flower-like, rod-like, and nanoparticle morphologies were equal to 56%, 50%, 46%, and 40%, respectively.

As can be seen in Fig. 9, the Fe/ZnO hollow sphere under visible light (after 60 min) was significantly efficient in removing dyes than other morphologies. While the efficiency of the Fe/ZnO hollow sphere for the CR and MB was 97% and 80%, respectively, the efficiency of wood-like reduced to 60% and 55%, respectively. The efficiency of flower-like, rod-like, and nanoparticle for degradation of CR was 53%, 49%, and 44%,

respectively. These values for MB were 49%, 46%, and 42%, respectively.

Consequently, all Fe/ZnO hollow spheres display higher photocatalytic activity than pure ZnO spheres. All the samples exhibit very high photocatalytic efficiency for the degradation of CR and MB solutions. The improvement in the efficiency of Fe/ZnO hollow spheres photocatalyst can be due to the synergistic effect between ZnO spheres and Fe/ZnO hollow spheres, resulting in the high activity of the Fe/ZnO hollow spheres photocatalysts. The formation of the vacant space in the center of spheres causes to the Fe/ZnO hollow spheres representing a large surface area (Fig. 10) [16]. The feasible mechanisms of photocatalytic degradation for the Fe/ZnO hollow spheres photocatalysts are suggested as follows [32]:

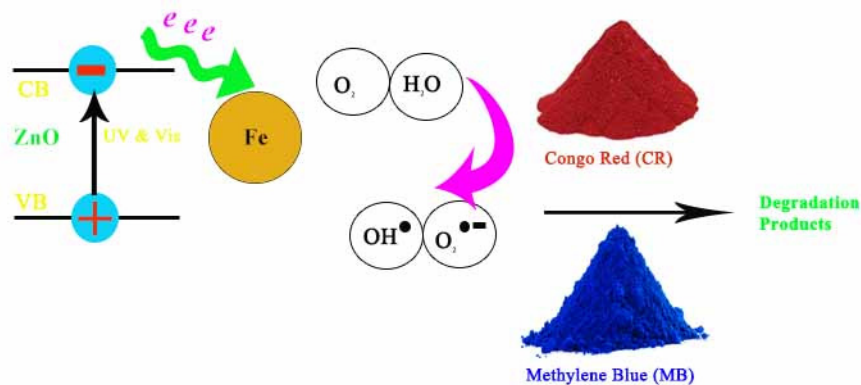
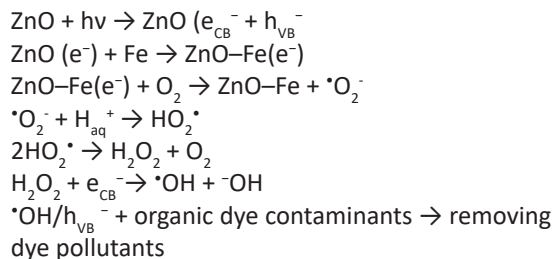


Fig. 10. Proposed mechanism for photodegradation of CR and MB by Fe/ZnO hollow spheres [32]

Table 1. Comparison of photocatalyst test results with similar ones in the literature.

Synthesis method	Pollutant	Time (min)	Photodegradation (%)	Ref.	Source
Precipitation method	Rhodamine (RhB)	100	97.7	[33]	UV light
Hydrothermal method	Tartrazine	180	96.5	[32]	UV light
Sonochemical method	Methylene Blue (MB) and Congo Red (CR)	35 60	83 (MB), 99 (CR) 80 (MB), 97 (CR)	This work	UV light Vis light



CONCLUSION

In the current research, we described an efficient strategy for the simple and green synthesis of x-Fe/ZnO hollow spheres (x = 0, 3, 5, and 10 wt %) as high-efficiency photocatalyst for the degradation of CR and MB dyes under UV-Vis light irradiations. Fructose was used for the synthesis of the carbon microspheres, which can be removed spontaneously to form the hollow core. The prepared Fe/ZnO nanostructure hollow spheres were characterized using FE-SEM-EDAX, XRD, and FT-IR analyses. In the presence of UV and visible light, the Fe/ZnO hollow spheres can simplify the degradation of these dyes. The outcomes demonstrate that Fe shows a key role in the transition of photogenerated charges in Fe/ZnO hollow spheres. Also, the results of the experiments confirmed that the synthesized

Fe/ZnO hollow spheres compared to other morphologies have excellent photocatalytic efficiency to the degradation of contaminants.

ACKNOWLEDGEMENTS

Author is grateful to the Farhangian University for supporting this work.

CONFLICT OF INTEREST

The authors declare that there is no conflict of interests regarding the publication of this manuscript.

REFERENCES

- Singh R, Kumar M, Khajuria H, Ladol J, Sheikh HN. Hydrothermal synthesis of magnetic Fe₃O₄-nitrogen-doped graphene hybrid composite and its application as photocatalyst in degradation of methyl orange and methylene blue dyes in presence of copper (II) ions. *Chemical Papers*. 2018;72(5):1181-92.
- Roonasi P, Mazinani M. Synthesis and application of barium ferrite/activated carbon composite as an effective solar photocatalyst for discoloration of organic dye contaminants in wastewater. *Journal of Environmental Chemical Engineering*. 2017;5(4):3822-7.
- Verma AK, Dash RR, Bhunia P. A review on chemical coagulation/flocculation technologies for removal of colour from textile wastewaters. *Journal of Environmental Management*. 2012;93(1):154-68.
- Golestaneh M. A simple and fast electrochemical nano-

- structure approach for the determination of Acid Red 52 in real samples. *Microchemical Journal*. 2020;158:105281.
5. Dai K, Peng X, Yang P, Li M, Tang C, Zhuang W, et al. Highly selective and efficient lignin-magnesium for removing cationic dyes from wastewater. *Journal of Environmental Chemical Engineering*. 2020;8(5):104283.
 6. Atallah E, Kwapinski W, Ahmad MN, Leahy JJ, Al-Muhtaseb AaH, Zeaiter J. Hydrothermal carbonization of olive mill wastewater: Liquid phase product analysis. *Journal of Environmental Chemical Engineering*. 2019;7(1):102833.
 7. Duan X, Wang X, Dai L, Feng L, Yan Y, Zhou Q. Simultaneous enhancement of nonylphenol biodegradation and short-chain fatty acids production in waste activated sludge under acidogenic conditions. *Science of The Total Environment*. 2019;651:24-31.
 8. Chávez AM, Gimeno O, Rey A, Pliego G, Oropesa AL, Álvarez PM, et al. Treatment of highly polluted industrial wastewater by means of sequential aerobic biological oxidation-ozone based AOPs. *Chemical Engineering Journal*. 2019;361:89-98.
 9. Xu J, Zhao L, Hou H, Guo H, Zhang H. Dependence of morphology, substrate and thickness of iron phthalocyanine thin films on the photocatalytic degradation of rhodamine B dye. *Chemical Papers*. 2018;72(9):2327-37.
 10. Golestaneh M (2019) Degradation of Organic Pollutant in Waste Water via CdMoO₄ Nanostructures as an Effective Photocatalyst; Ultrasound-assisted Preparation and Characterization. *J Nanostruct* 9:623-629.
 11. Chen X, Wu Z, Liu D, Gao Z. Preparation of ZnO Photocatalyst for the Efficient and Rapid Photocatalytic Degradation of Azo Dyes. *Nanoscale Research Letters*. 2017;12(1).
 12. Mishra J, Pattanayak DS, Das AA, Mishra DK, Rath D, Sahoo NK. Enhanced photocatalytic degradation of cyanide employing Fe-porphyrin sensitizer with hydroxyapatite palladium doped TiO₂ nano-composite system. *Journal of Molecular Liquids*. 2019;287:110821.
 13. Vaiano V, Iervolino G. Facile method to immobilize ZnO particles on glass spheres for the photocatalytic treatment of tannery wastewater. *Journal of Colloid and Interface Science*. 2018;518:192-9.
 14. Ong CB, Ng LY, Mohammad AW. A review of ZnO nanoparticles as solar photocatalysts: Synthesis, mechanisms and applications. *Renewable and Sustainable Energy Reviews*. 2018;81:536-51.
 15. Mousavi SM, Mahjoub AR, Abazari R. Green synthesis of ZnO hollow sphere nanostructures by a facile route at room temperature with efficient photocatalytic dye degradation properties. *RSC Advances*. 2015;5(130):107378-88.
 16. Yin Q, Qiao R, Zhu L, Li Z, Li M, Wu W. α -Fe₂O₃ decorated ZnO nanorod-assembled hollow microspheres: Synthesis and enhanced visible-light photocatalysis. *Materials Letters*. 2014;135:135-8.
 17. Bao C, Chen M, Jin X, Hu D, Huang Q. Efficient and stable photocatalytic reduction of aqueous hexavalent chromium ions by polyaniline surface-hybridized ZnO nanosheets. *Journal of Molecular Liquids*. 2019;279:133-45.
 18. Ahmad I, Akhtar MS, Ahmed E, Ahmad M. Facile synthesis of Pr-doped ZnO photocatalyst using sol-gel method and its visible light photocatalytic activity. *Journal of Materials Science: Materials in Electronics*. 2019;31(2):1084-93.
 19. Fox MA, Dulay MT. Heterogeneous photocatalysis. *Chemical Reviews*. 1993;93(1):341-57.
 20. Gao S, Jiao S, Lei B, Li H, Wang J, Yu Q, et al. Efficient photocatalyst based on ZnO nanorod arrays/p-type boron-doped-diamond heterojunction. *Journal of Materials Science: Materials in Electronics*. 2014;26(2):1018-22.
 21. Cho S, Jang J-W, Lee JS, Lee K-H. Porous ZnO-ZnSe nanocomposites for visible light photocatalysis. *Nanoscale*. 2012;4(6):2066.
 22. Wang X, Hu P, Fangli Y, Yu L. Preparation and Characterization of ZnO Hollow Spheres and ZnO-Carbon Composite Materials Using Colloidal Carbon Spheres as Templates. *The Journal of Physical Chemistry C*. 2007;111(18):6706-12.
 23. Kim S-W, Kim M, Lee WY, Hyeon T. Fabrication of Hollow Palladium Spheres and Their Successful Application to the Recyclable Heterogeneous Catalyst for Suzuki Coupling Reactions. *Journal of the American Chemical Society*. 2002;124(26):7642-3.
 24. Lou Z, Wang Y, Yang Y, Wang Y, Qin C, Liang R, et al. Carbon Sphere Template Derived Hollow Nanostructure for Photocatalysis and Gas Sensing. *Nanomaterials*. 2020;10(2):378.
 25. Zhu H, Jiang R, Xiao L, Chang Y, Guan Y, Li X, et al. Photocatalytic decolorization and degradation of Congo Red on innovative crosslinked chitosan/nano-CdS composite catalyst under visible light irradiation. *Journal of Hazardous Materials*. 2009;169(1-3):933-40.
 26. Mousavi SM, Mahjoub AR, Abazari R. Facile green fabrication of nanostructural Ni-doped ZnO hollow sphere as an advanced photocatalytic material for dye degradation. *Journal of Molecular Liquids*. 2017;242:512-9.
 27. Gabal MA, El-Bellihi AA, Ata-Allah SS. Effect of calcination temperature on Co(II) oxalate dihydrate-iron(II) oxalate dihydrate mixture. *Materials Chemistry and Physics*. 2003;81(1):84-92.
 28. Abazari R, Mahjoub AR, Saghatforoush LA, Sanati S. Characterization and optical properties of spherical WO₃ nanoparticles synthesized via the reverse microemulsion process and their photocatalytic behavior. *Materials Letters*. 2014;133:208-11.
 29. Li L, Han L, Han Y, Yang Z, Su B, Lei Z. Preparation and Enhanced Photocatalytic Properties of 3D Nanoarchitectural ZnO Hollow Spheres with Porous Shells. *Nanomaterials*. 2018;8(9):687.
 30. Ali MA, Idris MR, Quayum ME. Fabrication of ZnO nanoparticles by solution-combustion method for the photocatalytic degradation of organic dye. *Journal of Nanostructure in Chemistry*. 2013;3(1).
 31. Bordbar M, forghani-Pilerood S, Yeganeh-Faal A, Khodadadi B (2016) Effect of Morphology on the Photocatalytic Behavior of ZnO Nanostructures: Low-Temperature Sonochemical Synthesis of Ni Doped ZnO Nanoparticles. *J Nanostruct* 6:190-198.
 32. Türkyılmaz ŞŞ, Güy N, Özacar M. Photocatalytic efficiencies of Ni, Mn, Fe and Ag doped ZnO nanostructures synthesized by hydrothermal method: The synergistic/antagonistic effect between ZnO and metals. *Journal of Photochemistry and Photobiology A: Chemistry*. 2017;341:39-50.
 33. Hui A, Ma J, Liu J, Bao Y, Zhang J. Morphological evolution of Fe doped sea urchin-shaped ZnO nanoparticles with enhanced photocatalytic activity. *Journal of Alloys and Compounds*. 2017;696:639-47.